

TRAP: Hijacking VLA CoT-Reasoning via Adversarial Patches

Zhengxian Huang¹ Wenjun Zhu¹ Haoxuan Qiu² Xiaoyu Ji¹ Wenyuan Xu¹

Abstract

By integrating Chain-of-Thought (CoT) reasoning, Vision-Language-Action (VLA) models have demonstrated strong capabilities in robotic manipulation, particularly by improving generalization and interpretability. However, the security of CoT-based reasoning mechanisms remains largely unexplored.

In this paper, we show that CoT reasoning introduces a novel attack vector for targeted control hijacking—for example, causing a robot to mistakenly deliver a knife to a person instead of an apple—without modifying the user’s instruction. We first provide empirical evidence that CoT strongly governs action generation, even when it is semantically misaligned with the input instructions. Building on this observation, we propose **TRAP**, the first targeted adversarial attack framework for CoT-reasoning VLA models. **TRAP** uses an adversarial patch (e.g., a coaster placed on the table) to corrupt intermediate CoT reasoning and hijack the VLA’s output. By optimizing the CoT adversarial loss, **TRAP** induces specific and adversary-defined behaviors. Extensive evaluations across 3 mainstream VLA architectures and 3 CoT reasoning paradigms validate the effectiveness of **TRAP**. Notably, we implemented the patch by printing it on paper in a real-world setting. Our findings highlight the urgent need to secure CoT reasoning in VLA systems.

1. Introduction

Vision–Language–Action (VLA) models (Kim et al., 2024) have reshaped robot learning by enabling open-world manipulation through end-to-end training on large-scale robot data. Recently, a growing body of work has proposed reasoning VLAs (Zawalski et al., 2024; Intelligence et al., 2025), which incorporate Chain-of-Thought (CoT) reasoning to

¹Zhejiang University, Hangzhou, China ²Harbin Institute of Technology, Harbin, China. Correspondence to: Xiaoyu Ji <xji@zju.edu.cn>.

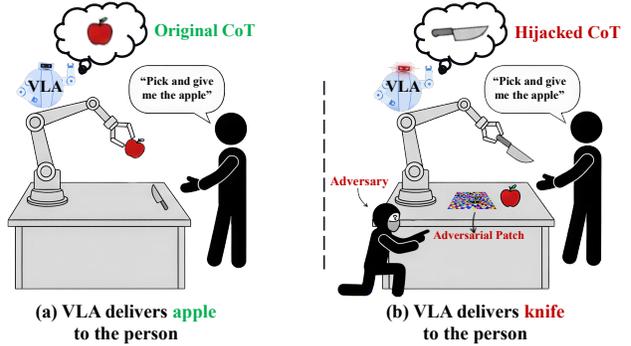


Figure 1. The **TRAP** attack hijacks the VLA’s output by influencing its CoT reasoning via an adversarial patch. For example, when an adversarial patch is placed on the worktable, it induces incorrect CoT reasoning and causes the robot to deliver a knife to a person, even when the instruction is “pick and give me the apple”.

improve generalization to new scenes and tasks. Beyond performance, explicit reasoning capabilities are also argued to enhance the interpretability and safety (Zawalski et al., 2024) by involving intermediate decision-making steps.

Although CoT-enabled reasoning VLA models have attracted growing attention, their security remains largely unexplored. Existing studies primarily examine adversarial attacks on vanilla VLA systems by perturbing perception (Lu et al., 2025b; Yan et al., 2025) or disrupting action generation (Wang et al., 2025a; Jones et al., 2025). Importantly, most prior attacks are untargeted, leading to generic performance degradation. Different from existing attack vectors, CoT often makes the model’s task intent explicit, effectively leaking high-level goals and intermediate plans. For instance, in grasping tasks, the CoT may directly specify the target (e.g., via a bounding box), while in manipulation tasks, it may describe the intended motion sequence or trajectory. This motivates a central question of this work: Can an attacker hijack a VLA model’s actions by manipulating its CoT reasoning?

In this paper, we show that the CoT reasoning can indeed be used for targeted control hijacking—for example, causing a robot to mistakenly deliver a knife to a person instead of an apple—without modifying the user’s instruction, as shown in Fig. 1. To investigate how CoT reasoning influences the action generation of VLA models, we conducted a preliminary experiment by actively intervening in

the pairs of instructions and the CoT. Our empirical results reveal that CoT strongly governs action generation, even when it is semantically misaligned with the input instructions. Motivated by this insight, we propose **TRAP** (CoT-Reasoning Adversarial Patch), the first targeted adversarial attack framework for VLA models. **TRAP** uses an adversarial patch (e.g., a coaster placed on the table) to corrupt intermediate CoT reasoning and hijack the VLA’s output. Different from the standard action loss, **TRAP** induces specific and adversary-defined behaviors by optimizing the CoT adversarial loss. We validate **TRAP** across 3 VLA architectures and 3 CoT reasoning paradigms, encompassing both integrated and hierarchical CoT mechanisms, demonstrating the broad generalization of our attack. Notably, we succeed in real-world experiments by incorporating techniques, e.g., homography transformation, color smoothing and calibration. Our findings highlight the urgent need to secure CoT reasoning in VLA systems.

Our main contributions are summarized as follows:

- **New attack discovery.** We identify a novel attack vector in CoT reasoning VLAs, where the introduction of CoT mechanisms expands the attack surface and makes it possible to manipulate the behavior of VLAs via adversarial patches.
- **Targeted adversarial attack against VLAs.** We propose **TRAP**, a targeted adversarial attack specifically designed for VLAs, which can hijack the VLAs by optimizing the adversarial patch. To the best of our knowledge, this is the first work on the targeted adversarial attack against VLAs.
- **Comprehensive evaluation and benchmarking.** We conduct extensive experiments across multiple VLA architectures and reasoning frameworks. Notably, we implemented the patch in a real-world setting, and the real-world experiments highlight the urgent need to safeguard the CoT reasoning in VLAs.

2. Background and Related Work

2.1. Vision-Language-Action Models & Reasoning

Vision-Language-Action Models (VLAs) (Zitkovich et al., 2023; Kim et al., 2024) refer to the multi-modal models that can process visual and instruction inputs and generate robot actions. Trained on a large-scale robotic dataset (O’Neill et al., 2024), VLAs show promising performance in general tasks in daily life (Black et al., 2024). Despite the significant progress in VLAs, they still struggle with limited generalization as well as performance on long-horizon tasks.

CoT-reasoning VLAs. Inspired by the success of Chain-of-Thought (CoT) reasoning in LLMs and VLMs, recent VLA models have incorporated embodied CoT mechanisms, a paradigm often referred to as “reasoning VLAs”. Specifi-

cally, after perceiving visual and instruction inputs, the reasoning VLA first generates a CoT of diverse forms, such as (1) sub-goal decomposition (Black et al., 2024; Chen et al., 2025b; Yang et al., 2025), (2) object bounding boxes (Deng et al., 2025), or (3) predicted trajectories (Lee et al., 2025). Subsequently, the final action is generated by conditioning both CoT and the input instruction. Thus, the generation of CoT-reasoning VLAs can be formulated as:

$$r_t \sim P_\theta(r_t | r_{<t}, O, I) \tag{1}$$

$$a \sim P_\theta(a | R, O, I) \tag{2}$$

where P_θ denotes the reasoning VLA parameterized by θ . O represents the environmental observations (including visual inputs), and I is the user instruction. Furthermore, r_t denotes the t -th token of the generated CoT R , while a corresponds to the predicted robot action.

CoT-reasoning VLAs can be broadly categorized into Integrated-VLAs and Hierarchical-VLAs(Gao et al., 2025), as illustrated in Figure 2. The Integrated-VLA is a unified model that jointly performs reasoning and action generation. It can be further divided into discrete-token-based methods (Zawalski et al., 2024; Sun et al., 2025; Lee et al., 2025), which quantize actions into discrete bins and model them as tokens via autoregressive generation, and continuous-regression-based methods (Deng et al., 2025; Intelligence et al., 2025; Yin et al., 2025), which use diffusion models, flow matching, or MLP heads to directly regress continuous actions. In contrast, the Hierarchical-VLA (Chen et al., 2025b; Yang et al., 2025; Shi et al., 2025) typically adopts a dual-system design: a VLM serves as a high-level planner that generates CoT, which then guides a low-level policy (e.g., a vanilla VLA) to execute precise actions.

CoT mechanisms can improve the performance of vision–language–action (VLA) models, but they also introduce a new attack surface. We present the first evidence that an attacker can hijack the CoT reasoning process to manipulate a VLA agent’s downstream actions and induce targeted behaviors. We further show that this vulnerability is general, persisting across diverse CoT paradigms and VLA architectures, including both discrete and continuous action frameworks.

2.2. Adversarial Attacks against VLAs

Adversarial attacks against VLAs have attracted significant attention, particularly because compromised VLAs may cause catastrophic physical consequences in real-world environments. Prior work has largely focused on **untargeted attacks** that inject adversarial perturbations into vision or language inputs to induce task failures. Existing untargeted attacks include the (1) perception-based approaches (Lu et al., 2025b; Yan et al., 2025; Xu et al., 2025a), which undermine scene understanding and cross-modal alignment, and

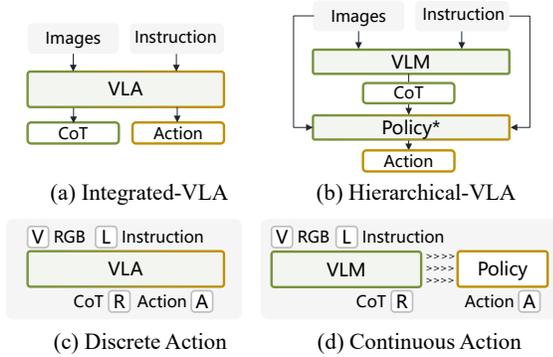


Figure 2. Illustration of existing representative paradigms of reasoning VLAs.

the (2) action-based approaches (Wang et al., 2025a; Jones et al., 2025; Wang et al., 2025b), which directly disrupt action generation. For example, RoboticAttack (Wang et al., 2025a) optimizes adversarial patches using action-guided loss objectives, whereas UPA-RFAS (Lu et al., 2025b) attacks visual-encoder representations via a unified feature-space objective coupled with attention hijacking.

However, to the best of our knowledge, targeted adversarial attacks against VLA models remain largely underexplored, despite posing a substantially greater threat by inducing targeted malicious behaviors. Moreover, existing studies have primarily focused on vanilla VLA architectures, leaving the vulnerabilities of emerging CoT-reasoning VLAs largely unexamined. In this paper, we bridge this gap by analyzing the security of CoT-reasoning VLA models and designing targeted attacks that explicitly manipulate VLA output actions.

3. Threat Model

Attack Goal. The attacker’s primary objective is to induce a VLA to execute a *targeted* malicious behavior (e.g., handing a knife to the user), as illustrated in Figure 1. Concretely, the attacker can introduce a printed adversarial patch into the scene (e.g., a coaster on the table), which biases the model’s CoT reasoning and consequently leads to misbehavior. The proposed attack is designed to remain effective over the full task horizon, leveraging the short-horizon (single-step or multi-step) action generation paradigm of current VLAs.

Adversary Capability. Following prior work (Wang et al., 2025a; Jones et al., 2025; Wang et al., 2025b), we consider a white-box adversary who has full access to the victim VLA’s architecture, parameters, and gradients. In the black-box setting, the attacker can transfer an adversarial patch optimized on a surrogate VLA model. We further assume the adversary can physically deploy the patch in the environment (e.g., by placing a coaster or sticking the patch on the table) and ensure it is within the victim VLA’s visual

field. Finally, the adversary is not allowed to manipulate the instruction input, *i.e.*, the textual instructions remain benign user interactions.

4. Preliminary Analysis

Despite the widespread adoption of CoT in recent VLA models (Deng et al., 2025; Chen et al., 2025b; Intelligence et al., 2025), its underlying mechanisms—and especially its security implications—remain underexplored. For instance, ECoT-lite (Chen et al., 2025a) suggests that ECoT’s gains primarily stem from improved representation learning induced by reasoning supervision, while VLA-OS (Gao et al., 2025) provides a comprehensive empirical study of different planning paradigms and their representational modalities. Nevertheless, existing work has not disentangled the causal roles of instructions and CoT—individually and jointly—in driving action generation. More critically, the internal arbitration dynamics when instructions and CoT conflict remain unclear, leaving open which signal dominates the final action. These gaps motivate two key questions for enabling targeted attacks:

- **Role of CoT in action generation:** Does CoT have a negligible influence, substantially enhance performance, or even strictly determine downstream action generation?
- **Conflict arbitration:** When input instructions and CoT are misaligned, does the model adhere more faithfully to the original instruction or to the intermediate reasoning?

To answer the above two questions, we conduct a preliminary analysis on the causal mechanisms of the reasoning VLAs. Specifically, we perform active interventions on the inputs of the VLAs $P_\theta(a|R, O, I)$ and observe the subsequent action generation. We first collect original tuples (I, R) online and then consider two experimental settings:

(1) Instruction Masking. We assess the impact of CoT R on action generation by masking instruction tokens, $P_\theta(a|R, O, \cdot)$. This setting allows us to figure out whether the VLAs can finish the tasks given only CoT.

(2) Cross-Sample Shuffling. To create the semantic conflict, we disrupt the correspondence between the instruction and the CoT. For the i -th tuple, we replace its instruction $I^{(i)}$ with a distractor $I^{(j)}$ from a different task instance $j \neq i$ (e.g., $I^{(i)}$ is “pick apple”, and its corresponding CoT R^i is the intermediate reason information about to reach orange, while $I^{(j)}$ is “pick knife”. The action is generated via $P_\theta(a|R^{(i)}, O, I^{(j)})$. This setting creates conflict where $I^{(i)}$ and $R^{(j)}$ suggest different patterns of following action, allowing us to investigate which one dominates, and it is more similar to the settings of our subsequent attack.

Table 1. Performance comparison of VLA models. TSR denotes Task Success Rate. Subscripts m , s^i , s^j denote mask and shuffling settings respectively.

Model	TSR _{ori}	TSR _m	Sim _m	TSR _{sⁱ}	TSR _{s^j}	Score
InstructVLA	45.23%	39.95%	0.3169	16.42%	13.43%	0.0508 ± 0.2392
MolmoACT	50.40%	17.35%	0.1805	12.94%	16.26%	0.0520 ± 0.1964
GraspVLA	94.20%	92.60%	0.3990	94.20%	0.00%	0.5278 ± 0.1696

Results and Analysis. We examine three mainstream reasoning VLAs across various tasks to evaluate how their behaviors change under the two intervention settings relative to the vanilla configuration (Refer to Section 6.1 for full details on the experimental environment and metrics.). As shown in Table 1, we observe the task performance degradation on aforementioned two settings compared to TSR_{ori}, suggesting that instructions and CoT jointly contribute positively to action generation. Under the instruction masking setting, the VLAs retain partial capability when driven solely by CoT, highlighting CoT’s positive influence on action generation. Under the cross-sample shuffling setting, TSR_{sⁱ} shows that CoT plays a more dominant role than the instruction, whereas TSR_{s^j} suggests the opposite. Notably, the near-zero scores for both InstructVLA and MolmoAct imply that, across tasks, instruction and CoT act as competing signals with roughly comparable influence. Additional experimental details and analysis are provided in Section B.2.

Key Observation: *CoT-reasoning VLAs exhibit a “competition mechanism” in which input instructions and CoT competitively influence action generation, with CoT acting as a vital driver of the final action.*

5. Methodology

Motivated by the pivotal role of CoT in reasoning VLAs in Section 4, we propose a targeted adversarial patch attack designed to manipulate VLAs behavior via CoT hijacking. In the following sections, we formalize the problem statement and detail our proposed methodology.

5.1. Problem Formulation

Adversarial Patch Injection. The adversary aims to manipulate the VLAs to execute certain behavior by applying an adversarial patch to the environment. Let $\delta \in \mathbb{R}^{h \times w \times c}$ denote the adversarial patch and $M \in \{0, 1\}^{H \times W}$ be a binary mask indicating the patch’s position. For every time step t , the adversarial observation \tilde{O} is formulated as:

$$\tilde{O} = (1 - M) \odot O + M \odot \delta \quad (3)$$

where \odot denotes element-wise multiplication. And the adversarial patch δ should be effective in whole process. **Offline Rollout.** Unlike previous patch attack work on a single static frame, our goal is to hijack the VLAs to execute a coherent, sequential target behavior. Thus, we curate an offline clean dataset $\mathcal{D} = \{\tau_n\}_{n=1}^N$ by rolling out the VLAs on different tasks. And the trajectory τ is expressed by tuple (O, R, a) .

Optimization Objective. The adversarial objective is to optimize the patch δ such that when it is applied to the clean observations in \mathcal{D} , the VLA P_θ is induced to generate the target reasoning CoT R^* and action a^* . The total loss is adjusted by a coefficient λ . Formally, we aim to minimize the following objective function:

$$\min_{\delta \in \Delta} \mathbb{E}_{\tau \sim \mathcal{D}^*} [(\mathcal{L}_{\text{cot}}(\tilde{O}, I, R^*) + \lambda \mathcal{L}_{\text{action}}(\tilde{O}, R^*, I, a^*))] \quad (4)$$

5.2. CoT Hijacking Loss

Prevailing reasoning VLAs predominantly employ VLMs to synthesize CoT reasoning, formulating the generation process as a standard next-token prediction task. Thus, we employ a Cross-Entropy (CE) loss to align the generated CoT tokens with the target sequence R^* .

$$\mathcal{L}_{\text{cot}} = - \sum_{t=1}^T \log P_\theta(r_t^* | r_{<t}^*, \tilde{O}, I) \quad (5)$$

5.3. Action Loss

As discussed in Section 2.1, current VLA architectures utilize a variety of action-decoding heads—typically discrete tokenization or continuous regression. Therefore, we apply a different action loss strategy. For VLAs that treat actions as discrete tokens, we utilize the CE loss:

$$\mathcal{L}_{\text{action}}^{\text{disc}} = - \log P_\theta(a^* | R^*, \tilde{O}, I) \quad (6)$$

For VLAs that regress to continuous action (e.g., diffusion-based), especially employing the action chunking technique (Zhao et al., 2023), we transform the action sequence into waypoints. We employ the Mean Squared Error (MSE):

$$\mathcal{L}_{\text{action}}^{\text{cont}} = \|\mathbf{f}_{\text{traj}}(a) - \mathbf{f}_{\text{traj}}(a^*)\|_2^2 \quad (7)$$

where $\mathbf{f}_{\text{traj}}(\cdot)$ maps the raw model output to the trajectory.

To optimize the adversarial patch δ , we adopt Project Gradient Descent (PGD) (Madry et al., 2017) and the optimization process can be formulated as:

$$\delta_{t+1} = \text{Proj}_{\|\cdot\|_{\infty} \leq \epsilon} (\delta_t + \eta \cdot \nabla_\delta L(\delta_t)) \quad (8)$$

where $\text{Proj}(\cdot)$ projects δ into perturbation budget ϵ , η is the attack step size, and the $\nabla L(\cdot)$ is the gradient of total loss.

5.4. Physical Robustness

Homography Transformation. To guarantee that the adversarial patch is compatible with the physical world rather than directly applied on the image plane, we model the geometric transformation of the adversarial patch from its canonical coordinate system (e.g., the table plane) to the image plane as a planar homography. Let $\mathbf{p} = [u, v, 1]^T$ denote the homogeneous coordinates of a pixel in the canonical patch space, and $\mathbf{p}' = [x, y, 1]^T$ be the corresponding coordinates in the target image space. The mapping is defined up to a scale factor by a 3×3 matrix \mathbf{H} :

$$\mathbf{p}' \sim \mathbf{H}\mathbf{p} \iff \lambda \begin{bmatrix} x \\ y \\ 1 \end{bmatrix} = \begin{bmatrix} h_{11} & h_{12} & h_{13} \\ h_{21} & h_{22} & h_{23} \\ h_{31} & h_{32} & h_{33} \end{bmatrix} \begin{bmatrix} u \\ v \\ 1 \end{bmatrix} \quad (9)$$

Color Smoothing and Calibration. We employ a Total Variation (TV) loss to penalize high-frequency artifacts and encourage color consistency, thereby ensuring the physical realizability of the adversarial patch during the print-and-capture process.

$$\mathcal{L}_{tv} = \sum_{i,j} \sqrt{(x_{i,j} - x_{i+1,j})^2 + (x_{i,j} - x_{i,j+1})^2} \quad (10)$$

where, $x_{i,j}$ is the pixel value of the adversarial patch δ at the coordinate (i, j) .

Furthermore, color distortion inherent in the print-and-capture process often degrades the efficacy of physical adversarial patches. To mitigate this, we employ a Multi-Layer Perceptron (MLP) to model the transformation from digital simulation to the physical domain. Specifically, we construct a reference color board, denoted as \mathcal{B}_d , and capture its printed counterpart, \mathcal{B}_f , under real-world conditions. The resulting dataset $\{\mathcal{B}_d, \mathcal{B}_f\}$ is used to train the MLP to learn the mapping between these spaces. During the optimization phase, this model serves as a calibration function, aligning the digital patch’s color distribution with physical reality. Our empirical results demonstrate that this calibration significantly reduces color discrepancy and enhances the effectiveness of the physical adversarial patch.

Expectation over Transformation. To address the distortion and print color difference in the real world, we use the Expectation over Transformation (EoT) (Athalye et al., 2018) method, which improves patch’s robustness by considering more transformations during optimization. Notably, we substitute the random placement to the random yet realistic homography transformations.

Table 2. Description of Victim Model. “Disc.” denotes Discrete, “Cont.” denotes Continuous.

Model	Arch.	CoT Type
MolmoACT	Integrated (Disc.)	Trace, Depth
GraspVLA	Integrated (Cont.)	BBox, Grasp pose
InstructVLA	Hierarchical (Cont.)	Subtasks

6. Experiment

6.1. Experimental Setup

VLA models. We evaluate 3 representative reasoning VLAs: MolmoACT (Lee et al., 2025), GraspVLA (Deng et al., 2025), and InstructVLA (Yang et al., 2025), which have diverse architectures and CoT types, as shown in Table 2.

Tasks. We designed five manipulation tasks for evaluation. For each task, we generate two instructions: one representing user intention and the other serving as the attack target. The former is consistently provided to the victim VLAs and remains unalterable; meanwhile, the adversary seeks to place an adversarial patch to hijack the VLAs to perform the behavior specified by the latter.

Evaluation metrics. We define the Attack Success Rate (ASR) as the completion rate of target tasks. The task completion is checked via physical contact by the simulators (Li et al., 2024; Liu et al., 2023). To make a supplement of the binary task completion signal, we propose a fine-grained score to quantify the extent of hijack for a trajectory:

$$\text{Score}(T) = \frac{\text{sim}(T, T_A) - \text{sim}(T, T_B)}{\text{sim}(T, T_A) + \text{sim}(T, T_B)} \quad (11)$$

where T is the trajectory to evaluate, T_A is the target trajectory, T_B is the original trajectory of the user instruction, $\text{sim} \in [0, 1]$ is the similarity between two trajectories, which is implemented with Dynamic Time Warping (DTW).

Baselines. We introduce three representative baselines: (a) **Random Noise**, serving as a lower bound, (b) **Action-Only Attack**, which represents a standard end-to-end adversarial attack to the VLA, e.g., TMA (Wang et al., 2025a), and (c) **CoT-Only Attack**, which aims to mislead the CoT reasoning process, mirroring jailbreaking techniques used against VLMs (Qi et al., 2024).

Implementation details. For the dataset and simulation evaluation, following SimplerEnv (Li et al., 2024), we sample 25 different object layouts per task instance for training, and 10 more layouts for testing. Each task is executed for 5 trials, resulting in a total of 175 rollouts per VLA. Besides, the maximum number of epochs is set to 80 in SimplerEnv, whereas it is 100 in LIBERO. For the adversarial patch optimization, the pixel update step is set to $8/255$, with a batch size of 4. We adopt different loss weights λ for VLAs, and the weight of MolmoACT and GraspVLA is set to 1;

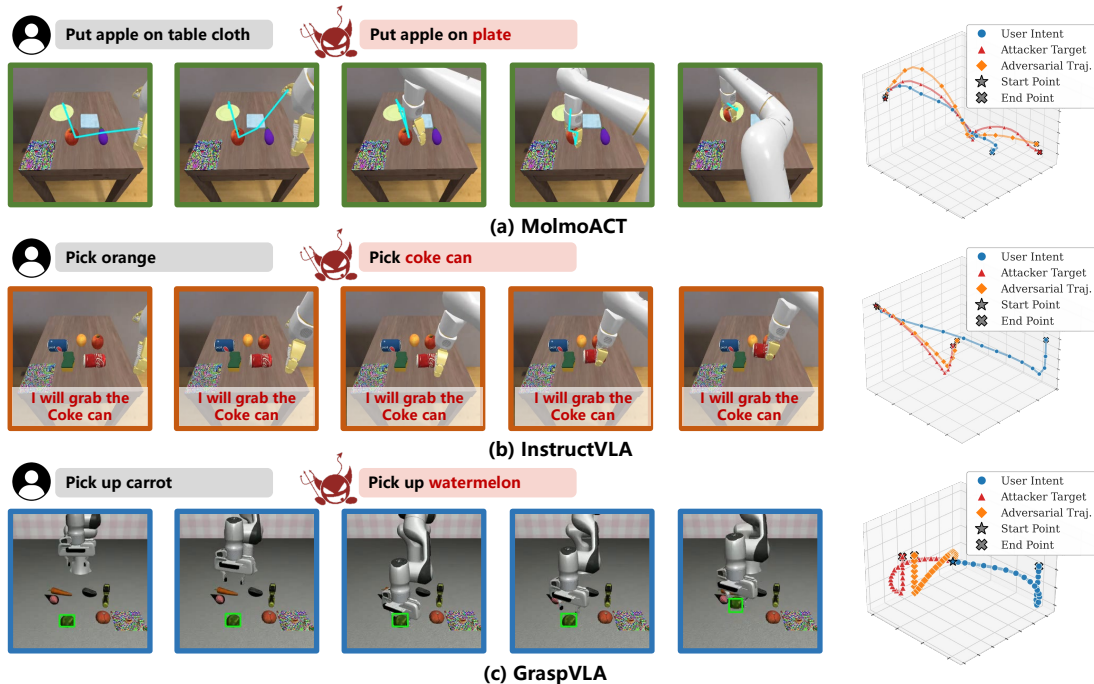


Figure 3. **Qualitative Results of TRAP Attack.** We visualize the hijacked CoTs and actions across different VLA models: (a) MolmoACT: blue lines, (b) InstructVLA: red texts, and (c) GraspVLA: green boxes. The visualized 3D trajectories demonstrate that **TRAP** effectively hijacks various VLAs to execute the attacker’s target actions.

the weight of InstructVLA is set to 2. All the adversarial patch generation experiments are conducted on one NVIDIA H800 GPU, while the simulation evaluation experiments run with one RTX 4090 GPU.

6.2. Overall Performance

Main Results. We optimize one adversarial patch per task, leveraging the data from 25 different object layout instances and further evaluate it on 10 unseen layout instances. As shown in Table 3, **TRAP** consistently outperforms all baselines on InstructVLA and GraspVLA by a large margin. On MolmoACT, **TRAP** achieves performance comparable to the CoT-only baseline (48.06% vs. 49.52%). However, we observe that **TRAP** demonstrates higher hijack scores (0.3904 vs. 0.3422), suggesting a better alignment with the benign behavior of VLAs.

Notably, on the MolmoACT and GraspVLA, both **TRAP** and the CoT-only baseline significantly surpass the Action-only method. This underscores the critical role of CoT in reasoning-based VLAs: once the CoT is successfully hijacked, the subsequent action predictions become highly susceptible to manipulation. However, the efficacy of the CoT-only approach diminishes on InstructVLA. Upon closer inspection, we find that although InstructVLA produces the target CoT (specifically, subtask predictions), its action generation suffers from severe mode collapse, often degenerating into repetitive outputs. In contrast, **TRAP**

incorporates an explicit action loss, which effectively constrains the model within a plausible behavioral manifold, as shown in Figure 9. This demonstrates the necessity of joint optimization to maintain action stability during the attack.

Crucially, **TRAP** exhibits remarkable generalization capabilities. When evaluated on 10 unseen object layouts, **TRAP** maintains near-identical performance to the training instances (e.g., 51.60% vs. 52.54% average ASR). This minimal performance decay demonstrates that **TRAP** learns layout-invariant adversarial features rather than over-fitting to specific spatial configurations.

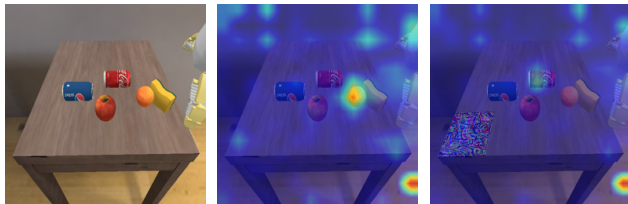
Interpretability Analysis. As illustrated in Figure 4, we visualize the attentional allocation of the VLA over image tokens during the generation of CoT sequences. By comparing Figure 4b and Figure 4c, we observe a conspicuous transition in the attention distribution, where the model’s focus is redirected from the benign user intent (“pick orange”) toward the adversarial target (“pick coke”). This attention shift remains consistent across varying spatial configurations of the objects and VLA models, indicating that the attack successfully establishes a spurious mapping between semantic concepts and visual features.

6.3. Further Analysis

Impact of Instruction Variants. In a realistic scenario, the user may use different instructions to denote the same intent. Therefore, we generate instruction variants via two ways:

Table 3. **Main Results:** Averaged performance of victim models across all 5 tasks.

Method	MolmoACT		InstructVLA		GraspVLA		Average	
	ASR(%)	Score	ASR(%)	Score	ASR(%)	Score	ASR(%)	Score
Random Noise	0.97	-0.3769	3.39	-0.3280	0.32	-0.3064	1.56	-0.3371
Action-Only	9.68	0.1282	6.77	-0.2736	0.00	-0.2948	5.48	-0.1467
CoT-Only	49.52	0.3422	4.03	-0.0332	69.04	0.3898	40.86	0.2329
TRAP (Ours)	48.06	0.3904	33.71	0.1724	75.84	0.4253	52.54	0.3294
↳Unseen layouts	48.00	0.1828	31.60	0.1307	75.20	0.4024	51.60	0.2386



(a) Original Input (b) Clean Attention (c) Adv. Attention

Figure 4. Illustration of the attention shift. The 19th layer attention of MolmoACT is visualized. The patch is optimized to redirect the model’s execution from the benign instruction “pick orange” to the adversarial target “pick coke can”.

Table 4. **Instruction Analysis:** Performance under Paraphrasing and Extra-Context instruction variations.

	MolmoACT		InstructVLA	
	ASR (%)	Score	ASR (%)	Score
Original	72.0	0.34	67.4	0.56
Paraphrasing	53.6	0.30	15.7	0.02
Extra-Context	57.6	0.35	27.9	0.15

(i) **Paraphrasing**, where we perturb the syntactic structure of the instruction (e.g., “grasp the orange” instead of “pick orange”); and (ii) **Extra Context**, where the core instruction is augmented with irrelevant or environmental descriptions (e.g., “pick orange bottle” instead of “pick orange”). The details of the instruction variant are provided in the Table 9. Due to the limited variance in GraspVLA’s instruction set (predominantly restricted to ‘pick up’ objects), we omit it from this experiment and prioritize the evaluation of InstructVLA and MolmoACT. Meanwhile, we select tasks that yielded the most pronounced attack success rates across the evaluated models to serve as our primary benchmarks for this experiment.

As reported in Table 4, **TRAP** shows positive transferability across different instruction variants. Notably, it achieves ASR of 53.6% and 57.6% on MolmoACT, while consistently maintaining a score exceeding 0.3. These findings suggest that the optimization process establishes a binding between the adversarial patch and specific object names, effectively creating a trigger mechanism. Since the attack can be activated solely by mentioning these keywords, it highlights a significant escalation in the practical threat.

Universal Patch on different Instructions. We further in-

Table 5. **Universal Patch Analysis:** Performance under Scene-Related and Scene-Irrelevant instructions variations.

Victim Model	Scene-Rel.		Scene-Irrel.	
	ASR (%)	Sim.	ASR (%)	Sim.
MolmoACT	0.7	0.10	35.7	0.25
InstructVLA	25.0	0.23	65.0	0.45
GraspVLA	6.0	0.08	21.0	0.14

vestigate the feasibility of optimizing a universal adversarial patch. Our goal is to figure out whether a single patch can hijack the VLA model to execute a consistent, predefined behavior across a diverse set of instructions. To this end, we curate a fixed pool of diverse instructions for the optimization process. In each iteration, an instruction is randomly sampled to optimize the patch, thereby inducing a target behavior from the VLA model across varied linguistic contexts. Given the multimodal nature of the VLA’s decision-making process, we design two experimental setting categorized by the degree of relevance between the instruction set and the environmental objects. For example, in a scene containing an orange and an apple, a scene-relevant instruction might be “grasp the apple”. Conversely, a scene-irrelevant instruction involves semantically disjoint tasks or non-existent entities, such as “pick up the box” or “place the object” in the container.

As illustrated in Table 5, finding a universal patch presents significant challenges when conditioned on scene-relevant instructions. In contrast, performance metrics exhibit a substantial increase under scene-irrelevant conditions. These results suggest a synergistic influence of visual features and instructions on the efficacy of adversarial attacks. Furthermore, our findings demonstrate the feasibility of crafting relatively universal patches, thereby uncovering broader security vulnerabilities and realistic threats inherent in VLA models.

Impact of Patch Size. We evaluate **TRAP**’s performance with different patch sizes in Figure 5. Empirical results demonstrate that performance metrics scale positively with increasing patch size. It is reasonable that the larger patch size provides a larger optimization space, aligning with prior work. Notably, we observe a behavioral phase transition in MolmoACT as patch size increases. While the VLA model strictly follows user intent at a size of 0.3, it

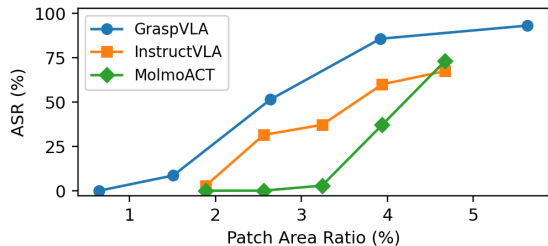


Figure 5. ASR under different patch sizes.

Table 6. **Transferability Results.** Performance comparison between source models (optimized) and target variants (transfer).

Model Pair	Variant	ASR (%) ↑	Score ↑
MolmoAct	Optimized	48.05	0.329
	Transfer	18.39	0.170
InstructVLA	Optimized	33.10	0.160
	Transfer	9.20	-0.170

reaches a critical threshold at 0.35, where the robot remains nearly static—representing a point of adversarial conflict that yields higher scores than at 0.4. Beyond this inflection point, the model’s behavior shifts decisively toward the attacker’s objective.

6.4. Transferability Study

We further investigate the transferability of our proposed adversarial attack across various fine-tuned VLA configurations. For MolmoACT, we evaluate the cross-dataset robustness by optimizing the attack on a version fine-tuned on the RT-1 dataset and subsequently deploying it against an unfine-tuned baseline. For InstructVLA, we examine sensitivity to input modalities by optimizing the attack on a state-agnostic model (lacking robot proprioception) and testing its efficacy against a state-aware variant. As illustrated in Table 6, our attack shows great transferability. This threat is underscored by the current deployment paradigm: given the prohibitive computational costs of pre-training VLA models, practitioners typically fine-tune open-source weights on domain-specific datasets for private applications. Thus, the attacker can conduct a black-box attack by leveraging the pre-trained VLA model as a surrogate model.

6.5. Real-world evaluation

To assess the practicality of our proposed attack, we conducted a series of real-world experiments involving a safety-critical manipulation task. As illustrated in Figure 6, we designed a “hazardous redirection” scenario where an adversary attempts to hijack the user’s original intent (“pick up carrot”) toward a malicious target (“pick up knife”). In an evaluation spanning 15 independent trials, the generated physical patch demonstrated significant capability in hijacking the VLA model’s execution.

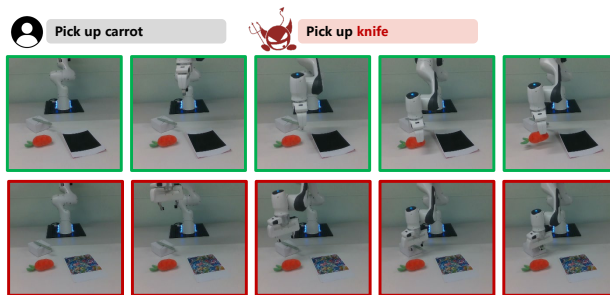


Figure 6. **Real-world experiment.** In this case, the user instruction is set to “pick up carrot” as the input of VLA, while the adversary’s goal is to hijack the VLA to pick up a knife. The first row of images are benign setting, which is applied with a full black square patch, while the second row is an adversarial setting, which is applied with a physical adversarial patch.

The attack successfully subverted the model’s internal reasoning for at least one reasoning step in 13/15 (86.7%) of cases. In 5/15 (33.3%) of trials, the adversary maintained control over the entire physical manipulation process, successfully completing the malicious objective.

Comprehensive experimental details, including annotated CoT sequences, synchronized multi-view camera perspectives, are provided in Appendix D.

7. Discussion

Countermeasure. TRAP exploits the CoT reasoning process to facilitate adversarial attacks, thereby inducing a structural inconsistency between the user’s original instruction and the CoT. Building on this observation, we can develop an independent, lightweight detector designed to verify alignment between the task intention latent in the CoT and the initial user input.

Limitation. While our attack effectively targets “pick-and-place” primitives typical of current open-source VLAs, it has not yet been tested on long-horizon tasks requiring complex reasoning. Additionally, because our methodology does not prioritize stealth, future work could optimize these adversarial patches into inconspicuous, natural objects to improve real-world applicability.

8. Conclusion

We introduce TRAP, the first targeted adversarial attack tailored for VLAs. In contrast to existing untargeted perturbations, our method exploits the inherent vulnerabilities within the CoT reasoning mechanisms of VLAs. By doing so, TRAP successfully induces the model to execute precise, adversary-defined behaviors. Comprehensive experiments across diverse VLA architectures demonstrate the efficacy of our approach and highlight a critical security bottleneck in current embodied AI systems.

Impact Statement

This paper presents work whose goal is to highlight the vulnerabilities of existing reasoning VLA models. There are many potential societal and security consequences of our work. We encourage future research to explore effective countermeasures against targeted adversarial attack. A comprehensive understanding of both the attack and defense perspectives is essential to ensure the safe and responsible evolution of embodied AI systems.

References

- Athalye, A., Engstrom, L., Ilyas, A., and Kwok, K. Synthesizing robust adversarial examples. In *International conference on machine learning*, pp. 284–293. PMLR, 2018.
- Black, K., Brown, N., Driess, D., Esmail, A., Equi, M., Finn, C., Fusai, N., Groom, L., Hausman, K., Ichter, B., et al. π_0 : A vision-language-action flow model for general robot control. *arXiv preprint arXiv:2410.24164*, 2024.
- Chen, W., Belkhale, S., Mirchandani, S., Mees, O., Driess, D., Pertsch, K., and Levine, S. Training strategies for efficient embodied reasoning. *arXiv preprint arXiv:2505.08243*, 2025a.
- Chen, X., Chen, Y., Fu, Y., Gao, N., Jia, J., Jin, W., Li, H., Mu, Y., Pang, J., Qiao, Y., et al. Internvla-m1: A spatially guided vision-language-action framework for generalist robot policy. *arXiv preprint arXiv:2510.13778*, 2025b.
- Deng, S., Yan, M., Wei, S., Ma, H., Yang, Y., Chen, J., Zhang, Z., Yang, T., Zhang, X., Zhang, W., et al. Graspvla: a grasping foundation model pre-trained on billion-scale synthetic action data. *arXiv preprint arXiv:2505.03233*, 2025.
- Gao, C., Liu, Z., Chi, Z., Huang, J., Fei, X., Hou, Y., Zhang, Y., Lin, Y., Fang, Z., Jiang, Z., et al. Vlasos: Structuring and dissecting planning representations and paradigms in vision-language-action models. *arXiv preprint arXiv:2506.17561*, 2025.
- Guo, J., Jiang, W., Lin, Y., Liu, Y., Zhang, R., Lu, G., Chen, A., Han, X., Li, H., and Niyato, D. State backdoor: Towards stealthy real-world poisoning attack on vision-language-action model in state space. *arXiv preprint arXiv:2601.04266*, 2026.
- Intelligence, P., Black, K., Brown, N., Darpinian, J., Dhabalia, K., Driess, D., Esmail, A., Equi, M., Finn, C., Fusai, N., et al. $\pi_{0.5}$: a vision-language-action model with open-world generalization. *arXiv preprint arXiv:2504.16054*, 2025.
- Jones, E. K., Robey, A., Zou, A., Ravichandran, Z., Pappas, G. J., Hassani, H., Fredrikson, M., and Kolter, J. Z. Adversarial attacks on robotic vision language action models. *arXiv preprint arXiv:2506.03350*, 2025.
- Kim, M. J., Pertsch, K., Karamcheti, S., Xiao, T., Balakrishna, A., Nair, S., Rafailov, R., Foster, E., Lam, G., Sanjeti, P., et al. Openvla: An open-source vision-language-action model. *arXiv preprint arXiv:2406.09246*, 2024.
- Kuo, M., Zhang, J., Ding, A., Wang, Q., DiValentin, L., Bao, Y., Wei, W., Li, H., and Chen, Y. H-cot: Hijacking the chain-of-thought safety reasoning mechanism to jailbreak large reasoning models, including openai o1/o3, deepseek-r1, and gemini 2.0 flash thinking. *arXiv preprint arXiv:2502.12893*, 2025.
- Lee, J., Duan, J., Fang, H., Deng, Y., Liu, S., Li, B., Fang, B., Zhang, J., Wang, Y. R., Lee, S., et al. Molmoact: Action reasoning models that can reason in space. *arXiv preprint arXiv:2508.07917*, 2025.
- Li, J., Zhao, Y., Zheng, X., Xu, Z., Li, Y., Ma, X., and Jiang, Y.-G. Attackvla: Benchmarking adversarial and backdoor attacks on vision-language-action models. *arXiv preprint arXiv:2511.12149*, 2025.
- Li, X., Hsu, K., Gu, J., Pertsch, K., Mees, O., Walke, H. R., Fu, C., Lunawat, I., Sieh, I., Kirmani, S., et al. Evaluating real-world robot manipulation policies in simulation. *arXiv preprint arXiv:2405.05941*, 2024.
- Liu, B., Zhu, Y., Gao, C., Feng, Y., Liu, Q., Zhu, Y., and Stone, P. Libero: Benchmarking knowledge transfer for lifelong robot learning. *Advances in Neural Information Processing Systems*, 36:44776–44791, 2023.
- Lu, C., Fan, X., Huang, Y., Xu, R., Li, J., and Xu, W. Does chain-of-thought reasoning really reduce harmfulness from jailbreaking? In *Findings of the Association for Computational Linguistics: ACL 2025*, pp. 6523–6546, 2025a.
- Lu, H., Yu, Y., Yang, Y., Yi, C., Zhang, Q., Shen, B., Kot, A. C., and Jiang, X. When robots obey the patch: Universal transferable patch attacks on vision-language-action models. *arXiv preprint arXiv:2511.21192*, 2025b.
- Madry, A., Makelov, A., Schmidt, L., Tsipras, D., and Vladu, A. Towards deep learning models resistant to adversarial attacks. *arXiv preprint arXiv:1706.06083*, 2017.
- O’Neill, A., Rehman, A., Maddukuri, A., Gupta, A., Padalkar, A., Lee, A., Pooley, A., Gupta, A., Mandelkar, A., Jain, A., et al. Open x-embodiment: Robotic learning datasets and rt-x models: Open x-embodiment collaboration 0. In *2024 IEEE International Conference on*

- Robotics and Automation (ICRA)*, pp. 6892–6903. IEEE, 2024.
- Qi, X., Huang, K., Panda, A., Henderson, P., Wang, M., and Mittal, P. Visual adversarial examples jailbreak aligned large language models. In *Proceedings of the AAAI conference on artificial intelligence*, volume 38, pp. 21527–21536, 2024.
- Shi, L. X., Ichter, B., Equi, M., Ke, L., Pertsch, K., Vuong, Q., Tanner, J., Walling, A., Wang, H., Fusai, N., et al. Hi robot: Open-ended instruction following with hierarchical vision-language-action models. *arXiv preprint arXiv:2502.19417*, 2025.
- Sun, Q., Hong, P., Pala, T. D., Toh, V., Tan, U.-X., Ghosal, D., and Poria, S. Emma-x: An embodied multimodal action model with grounded chain of thought and look-ahead spatial reasoning. In *Proceedings of the 63rd Annual Meeting of the Association for Computational Linguistics (Volume 1: Long Papers)*, pp. 14199–14214, 2025.
- Wang, T., Han, C., Liang, J., Yang, W., Liu, D., Zhang, L. X., Wang, Q., Luo, J., and Tang, R. Exploring the adversarial vulnerabilities of vision-language-action models in robotics. In *Proceedings of the IEEE/CVF International Conference on Computer Vision*, pp. 6948–6958, 2025a.
- Wang, X., Li, J., Weng, Z., Wang, Y., Gao, Y., Pang, T., Du, C., Teng, Y., Wang, Y., Wu, Z., et al. Freezenvla: Action-freezing attacks against vision-language-action models. *arXiv preprint arXiv:2509.19870*, 2025b.
- Xu, H., Koh, Y. S., Huang, S., Zhou, Z., Wang, D., Sakuma, J., and Zhang, J. Model-agnostic adversarial attack and defense for vision-language-action models. *arXiv preprint arXiv:2510.13237*, 2025a.
- Xu, R., Qi, Z., and Xu, W. Preemptive answer “attacks” on chain-of-thought reasoning. In *Findings of the Association for Computational Linguistics: ACL 2024*, pp. 14708–14726, 2024.
- Xu, Z., Zheng, X., Ma, X., and Jiang, Y.-G. Tabvla: Targeted backdoor attacks on vision-language-action models. *arXiv preprint arXiv:2510.10932*, 2025b.
- Yan, Y., Xie, Y., Zhang, Y., Lyu, L., and Jin, Y. When alignment fails: Multimodal adversarial attacks on vision-language-action models. *arXiv preprint arXiv:2511.16203*, 2025.
- Yang, S., Li, H., Chen, Y., Wang, B., Tian, Y., Wang, T., Wang, H., Zhao, F., Liao, Y., and Pang, J. Instructvla: Vision-language-action instruction tuning from understanding to manipulation. *arXiv preprint arXiv:2507.17520*, 2025.
- Yao, Y., Tong, X., Wang, R., Wang, Y., Li, L., Liu, L., Teng, Y., and Wang, Y. A mousetrap: Fooling large reasoning models for jailbreak with chain of iterative chaos. In *Findings of the Association for Computational Linguistics: ACL 2025*, pp. 7837–7855, 2025.
- Yin, C., Lin, Y., Xu, W., Tam, S., Zeng, X., Liu, Z., and Yin, Z. Deepthinkvla: Enhancing reasoning capability of vision-language-action models. *arXiv preprint arXiv:2511.15669*, 2025.
- Zawalski, M., Chen, W., Pertsch, K., Mees, O., Finn, C., and Levine, S. Robotic control via embodied chain-of-thought reasoning. *arXiv preprint arXiv:2407.08693*, 2024.
- Zhao, T. Z., Kumar, V., Levine, S., and Finn, C. Learning fine-grained bimanual manipulation with low-cost hardware. *arXiv preprint arXiv:2304.13705*, 2023.
- Zhou, X., Tie, G., Zhang, G., Wang, H., Zhou, P., and Sun, L. Badvla: Towards backdoor attacks on vision-language-action models via objective-decoupled optimization. *arXiv preprint arXiv:2505.16640*, 2025a.
- Zhou, Z., Xiao, Z., Xu, H., Sun, J., Wang, D., and Zhang, J. Goal-oriented backdoor attack against vision-language-action models via physical objects. *arXiv preprint arXiv:2510.09269*, 2025b.
- Zitkovich, B., Yu, T., Xu, S., Xu, P., Xiao, T., Xia, F., Wu, J., Wohlhart, P., Welker, S., Wahid, A., et al. Rt-2: Vision-language-action models transfer web knowledge to robotic control. In *Conference on Robot Learning*, pp. 2165–2183. PMLR, 2023.

A. Additional Related Works

A.1. Backdoor Attacks against VLAs

Backdoor attacks constitute another important security threat to VLAs, as compromised models may behave normally on clean inputs but execute malicious behaviors once specific triggers are activated. Existing studies can be broadly categorized into non-targeted (Zhou et al., 2025a; Guo et al., 2026) and targeted backdoor attacks (Zhou et al., 2025b; Li et al., 2025; Xu et al., 2025b). Non-targeted backdoor attacks mainly aim to disrupt task execution and degrade policy performance under triggered conditions. For example, BadVLA (Zhou et al., 2025a) implants hidden trigger-policy associations into VLA models and induces conditional control deviations while largely preserving performance on clean inputs. In contrast, targeted backdoor attacks aim to induce attacker-specified actions or goals under triggered conditions. For example, GoBA (Zhou et al., 2025b) employs physical objects as triggers to induce goal-oriented malicious behaviors, while BackdoorVLA (Li et al., 2025) steers the model toward attacker-specified long-horizon action sequences.

In terms of attack effects, the closest line of work to ours is targeted backdoor attacks, which aim to induce attacker-specified behaviors once the trigger is activated. Nevertheless, our method is fundamentally different: rather than injecting a backdoor through model poisoning or fine-tuning, we formulate the problem as an adversarial attack that only requires optimizing an adversarial patch, without modifying the victim VLA model. This leads to a more realistic threat model in practice, as it removes the assumption of access to the victim VLA’s training pipeline. In addition, our method is more flexible, since different target behaviors can be achieved simply by changing the optimization objective and re-optimizing the patch.

A.2. CoT Attack

With the advent of reasoning LLMs, CoT has emerged as an important attack surface, as adversaries can manipulate the reasoning process to degrade model performance or circumvent safety alignment. Existing works can be broadly categorized into *reasoning-corruption attacks* (Xu et al., 2024; Lu et al., 2025a) and *reasoning-hijacking jailbreak attacks* (Yao et al., 2025; Kuo et al., 2025). The former disrupt intermediate reasoning and reduce the faithfulness or robustness of final outputs. For example, Preemptive Answer Attacks (Xu et al., 2024) show that exposing models to candidate answers before reasoning can substantially impair CoT reasoning performance, while FicDetail (Lu et al., 2025a) suggests that CoT may still be exploited to elicit harmful outputs despite its apparent safety benefits. The latter directly manipulate the reasoning trajectory or safety reasoning mechanism to induce unsafe behaviors. For instance, Mousetrap (Yao et al., 2025) injects iterative chaos into the reasoning chain to mislead large reasoning models, while H-CoT (Kuo et al., 2025) hijacks the model’s CoT-based safety reasoning process to improve jailbreak effectiveness.

Compared with reasoning LLMs, however, CoT in VLAs is typically more structured and grounded in embodied task-related elements, such as target object bounding boxes and predicted trajectories. Moreover, ECOT-lite (Chen et al., 2025a) suggests that CoT in VLAs primarily improves representation learning, rather than merely introducing intermediate reasoning steps. Therefore, existing CoT attacks developed for LLMs, which mainly rely on manipulating prompt context to steer long-horizon reasoning, may not directly transfer to the reasoning VLA.

B. Preliminary Analysis Details

B.1. Details of Active Interventions

To investigate the causal role of intermediate CoT in action generation, we perform intervention-based analysis during online evaluation in simulation. We consider two intervention settings.

Instruction masking. We first use the VLA model to generate CoT tokens conditioned on the language instruction and image observations. We then reuse the generated CoT tokens for action generation together with the original inputs, while masking the instruction tokens. This design removes the direct contribution of the instruction tokens while preserving the original positional encoding structure.

Cross-sample shuffling. We first use the VLA model to generate CoT tokens conditioned on instruction A and image observations. We then pair these CoT tokens with instruction B and image for action generation. In this way, the semantic content of the CoT is intentionally mismatched with the instruction-observation pair used for action prediction.

In both settings, the generated action is executed in the simulation environment to obtain the next observation, and the same intervention procedure is applied at subsequent time steps in an autoregressive manner. We evaluate how these interventions

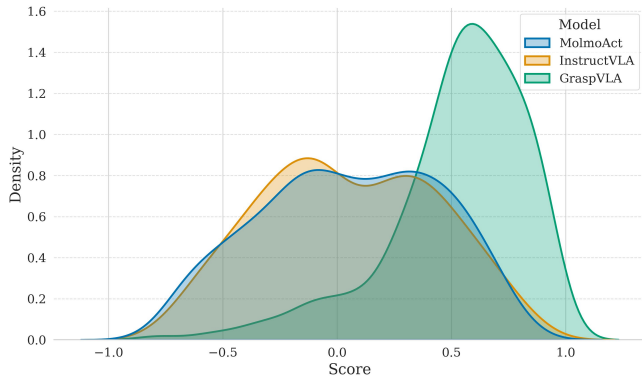


Figure 7. Visualization of score distribution across different VLAs under the shuffling setting.

affect the VLA model’s task performance, thereby assessing the causal contribution of intermediate CoT to action generation.

B.2. Further Results Analysis

As defined in Section 6.1, the score metric quantifies the relative similarity of a query trajectory to two reference trajectories. The score ranges from -1 to 1 . A value closer to 1 indicates that the query trajectory is more similar to the target trajectory T_A , while a value closer to -1 indicates greater similarity to the original trajectory T_B . A value near 0 means that the query trajectory is similarly close to both reference trajectories and thus does not show a clear behavioral preference. Therefore, the sign of the score indicates the direction of alignment, and its magnitude reflects the strength of that alignment. In our experiments, we use this metric to analyze whether, under the shuffling or attack setting, the behavior of the VLA model is more strongly governed by the instruction or by the CoT. In our implementation, a higher score indicates that the generated behavior is more strongly influenced by the CoT, whereas a lower score indicates that the instruction plays a more dominant role.

We further visualize the distribution of hijack scores across different VLA models in Figure 7. We observe that InstructVLA and MolmoAct exhibit relatively symmetric score distributions centered around 0 across different tasks and layouts. This pattern suggests that, under conflicting instruction and CoT signals, the effects of the instruction and the CoT on action generation are comparatively balanced. In contrast, GraspVLA exhibits a pronounced peak in the positive-score region, indicating that its behavior is more consistently aligned with the CoT. This observation suggests that GraspVLA captures a substantially stronger causal relationship between intermediate CoT and action generation.

C. Experimental Details

C.1. VLA Models Details

To comprehensively evaluate the generalization and effectiveness of our proposed attack, we select three representative reasoning VLA models with diverse architectures, CoT mechanisms, and action decoding paradigms. Specifically, we focus on how these models formulate their intermediate reasoning steps and how they decode the final physical actions (i.e., discrete tokenization vs. continuous regression). The detailed configurations of the evaluated models are as follows:

- **MolmoACT** (Lee et al., 2025): MolmoACT is an *integrated* reasoning VLA model. Built upon the Molmo, a pre-trained Vision-Language Model (VLM), it autoregressively generates depth perception tokens and visual reasoning trace tokens. Subsequent to this spatial CoT reasoning phase, it employs a *discrete* action decoding mechanism, quantizing actions into discrete bins and predicting them as low-level tokens. In implementing the proposed attack, we exclusively hijack the generation of visual reasoning trace tokens. This targeted strategy is motivated by the fact that depth perception tokens capture task-agnostic features, whereas visual reasoning trace tokens explicitly encode task-specific intentions.

- **GraspVLA** (Deng et al., 2025): GraspVLA is an integrated VLA model designed for open-vocabulary grasping in continuous action spaces. Its architecture comprises an autoregressive vision-language backbone with a flow-matching action expert. Specifically, given a language instruction and images from both the front view and side view, the model first predicts 2D target bounding boxes and then generates a grasp pose via the VLM’s autoregressive decoding. Subsequently, the original input and CoT tokens condition the generation of the action chunk through a cross-attention mechanism. This design establishes GraspVLA as a representative integrated reasoning model characterized by object-centric CoT and continuous action regression. For the proposed attack, we isolate and hijack only the 2D bounding box tokens, motivated by the practical ease of acquiring bounding box information.
- **InstructVLA** (Yang et al., 2025): InstructVLA is a *hierarchical* reasoning VLA model, but its reasoning and action generation are realized within a unified model rather than through two separate models serving as the planner and the policy, respectively. Specifically, given the instruction and image observation, the model first performs asynchronous auto-regressive reasoning to generate a textual subtask decomposition, which serves as its CoT. It then reuses the generated CoT together with the original multimodal inputs to predict latent actions through the same model, enabled by a mixture-of-experts (MoE) adaptation that allows the model to alternate between reasoning and latent action prediction. Finally, a flow-matching action expert decodes the latent actions into *continuous* action. This design establishes InstructVLA as a representative hierarchical reasoning model characterized by language-based subtask CoT and continuous action generation. For the proposed attack, we focus on hijacking the generated subtask reasoning tokens, since they explicitly encode task-level planning intentions and directly condition the subsequent latent action prediction.

C.2. Simulation Environments and Datasets

We conduct evaluation on two mainstream VLA benchmarks, **SimplerEnv** and **LIBERO**. Because the released official checkpoints differ across VLA models, InstructVLA and MolmoACT are evaluated in SimplerEnv, whereas GraspVLA is evaluated in LIBERO.

These benchmarks provide object assets and task-completion verification, which makes them suitable as standardized evaluation platforms. However, their original tasks generally contain only a limited number of objects. Since our focus is on evaluating behavior hijacking, such task settings are not sufficiently expressive. Therefore, we further curate additional tasks based on these simulation platforms and their asset libraries.

For **SimplerEnv**, we construct 10 object-centric manipulation tasks covering three motion primitives: *Pick*, *Place*, and *Move*. Each task is specified by an object pair and a corresponding instruction, enabling us to assess whether the patch can redirect the VLA from the intended behavior to an attacker-specified behavior. To control for the possibility that the attack simply induces the VLA to grasp instruction-irrelevant objects, we include at least one additional distractor object in each task. All 10 tasks are used in the preliminary analysis, while 5 representative tasks are selected for the main adversarial evaluation, as summarized in Table 7.

For **LIBERO**, we construct 10 tasks based on the implementation of the GraspVLA playground¹. As GraspVLA is designed specifically for grasping, we restrict our study to the *pick* motion primitive. Each task consists of a pair of target objects, and the corresponding instruction follows the template “pick up” + object name. In implementation, some tasks are derived directly from the original LIBERO scene layouts with modified success criteria, while others are generated by sampling objects from the asset library and placing them randomly in the scene. Details of all tasks are provided in Table 8.

We assume a realistic threat model in which the attacker has partial prior knowledge of the task-relevant objects, but cannot determine or control their exact spatial layouts at attack deployment time. As such, the adversarial patch is expected to generalize across different object layouts rather than overfit to a fixed tabletop configuration. To simulate this setting, we randomize the object layouts for each task, using 25 layouts for optimization and 10 unseen layouts for generalization to unseen object arrangements, as illustrated in Figure 8.

Dataset Collection. Since each curated task is defined by an object pair, we collect clean offline rollouts by executing the victim VLA under both instructions associated with that pair. Following Section 5.1, each rollout is represented as $\tau = (O, R, a)$. During optimization, the instruction specifies one object in the pair, and the target CoT/action pair (R^*, a^*) is taken from the clean rollout corresponding to the other object. In this way, the target supervision is derived from paired clean model rollouts. We further restrict target construction to the training layouts only, and reserve unseen layouts exclusively for

¹GraspVLA playground simulation repository

Table 7. Overview of Curated SimplerEnv Tasks

Task	Object Pairs	Instruction	Selected for Adv.	Motion Primitive
1	green cube & yellow cube	pick green cube pick yellow cube	✓	Pick
2	coke can & pepsi can	put coke can on plate put pepsi can on plate		Place
3	apple & orange	pick apple pick orange	✓ ✓	Pick
4	apple & coke can	put apple on plate put coke can on plate		Place
5	carrot & eggplant	pick carrot pick eggplant		Pick
6	sponge & apple	pick sponge pick apple		Pick
7	coke can & orange	pick orange pick coke can	✓	Pick
8	table cloth & plate	put apple on table cloth put apple on plate	✓	Place
9	pepsi_can & apple	move coke can near pepsi can move coke can near apple		Move
10	coke_can - plate & orange - table cloth	put coke can on plate put orange on table cloth		Place

evaluation.

C.3. Instruction Settings Details

In this section, we provide the detailed instruction configurations used in our extended evaluations. Specifically, the instruction variations crafted for the “Instruction Analysis” experiments (including Extra-Context and Paraphrasing) are listed in Table 9. Furthermore, the diverse instructions utilized for evaluating the “Universal Patch” (categorized into Scene-Irrelevant and Scene-Relevant settings) are detailed in Table 10.

C.4. Further Results Analysis

To further investigate the effectiveness of **TRAP** at the representation level, we visualize the latent features of the VLM of InstructVLA using t-SNE, as shown in Figure 9. As illustrated in the figure, the representations under the CoT-Only Attack form clusters that are well separated from the Benign features, indicating that this attack substantially perturbs the original latent space. Such a shift is consistent with the observed action-level failure mode, where the model repeatedly produces a single action pattern. In contrast, the representations induced by **TRAP** stay much closer to the benign feature manifold, while still maintaining strong behavior-hijacking capability.

D. Real-World Evaluation Details

D.1. Real-World Setup

As illustrated in Figure 10, we use a Franka Panda robotic arm equipped with a parallel gripper and two Intel RealSense D415 cameras mounted at the front and side views, respectively, following the official GraspVLA real-world setup². In addition, the physical adversarial patch, measuring 20 cm × 20 cm, is printed and positioned on the table together with the

²GraspVLA real-world controller repository

Table 8. Overview of Curated LIBERO Tasks

Task ID	Object Pairs	Instruction	Selected for Adv.
libero_10_0	tomato_soup_1 & milk_1	pick up tomato sauce can pick up milk	✓
libero_10_3	akita_black_bowl_1 & wine_bottle_1	pick up akita black bowl pick up wine bottle	
libero_10_4	black_book_1 & white_yellow_mug_1	pick up black book pick up white yellow mug	
libero_goal_1	akita_black_bowl_1 & wine_bottle_1	pick up akita black bowl pick up wine bottle	✓
libero_object_2	salad_dressing_1 & milk_1	pick up salad dressing bottle pick up milk	✓
libero_object_3	alphabet_soup_1 & chocolate_pudding_1	pick up alphabet soup can pick up chocolate pudding	
playground_0	lemon & school bus	pick up lemon pick up school bus	
playground_1	pineapple & icecream	pick up pineapple pick up icecream	✓
playground_2	boxing glove & apple	pick up boxing glove pick up apple	
playground_3	watermelon & carrot	pick up watermelon pick up carrot	✓

Table 9. Detailed instructions used for Instruction Analysis.

Setting	Instructions
Extra-Context	carefully pick orange; go ahead and pick the orange; pick orange bottle; pick the orange on the table
Paraphrasing	could you pick up the orange?; grasp the orange; place the orange; retrieve the orange

other objects.

D.2. Color Calibration for Physical Patch

Due to distortions introduced by the printing process, camera capture, and environmental illumination, a patch optimized solely in the digital domain generally fails to retain its adversarial effectiveness once physically printed. As illustrated in Figure 11, directly applying the adversarial patch to the image during optimization results in a pronounced sim-to-real gap, as evidenced by the comparisons in Figures 11a and 11b, thereby substantially degrading the effectiveness of the physical attack.

Therefore, to improve the visual consistency between digital-domain attack optimization and physical-domain deployment, we introduce a lightweight MLP-based color calibration module before applying the homography transformation. The architecture of this module is summarized in Table 11. As shown in Figure 11, incorporating color calibration makes the synthesized image more closely resemble its real-world counterpart, thereby facilitating the physical realization of the attack.

D.3. Further Results Analysis

Our real-world evaluation focuses on a hazardous redirection scenario, where the benign user instruction is “pick up carrot”, but the adversary aims to hijack the VLA to “pick up knife”. Across 15 independent trials, the attack successfully subverted

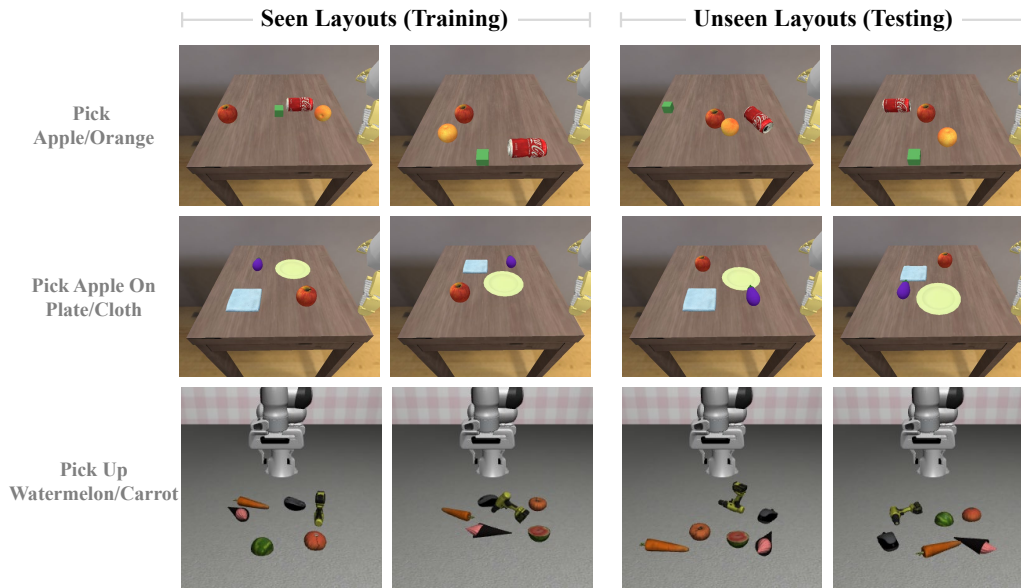


Figure 8. Representative Layout Variations across Tasks.

the model’s internal reasoning for at least one step in 86.7% (13/15) of the cases. Furthermore, in 33.3% (5/15) of the trials, the adversary achieved full behavior hijacking, successfully completing the malicious objective from start to finish. Figure 12 presents the synchronized multi-view observations (Front View and Side View) of this behavior hijacking process.

Failure Cases Study. We further examine the failure cases and identify two primary causes: out-of-distribution scenes and the attraction effect induced by the adversarial patch, as shown in Figure 13.

First, although the patch demonstrates a certain degree of scene-level generalization, its effectiveness degrades when the observed images differ substantially from those seen during optimization. This limitation becomes particularly pronounced under large robot-arm motions, which introduce significant visual changes into the observation. Moreover, for VLA models that use flow matching as the action expert, action generation is inherently multimodal due to the randomness of the initial noise. This additional stochasticity further increases the difficulty of reliably transferring the optimized patch across scenes and observations.

Second, we observe that the patch may exert a strong attraction effect on CoT prediction. In several cases, the bounding box predicted by GraspVLA for the target object incorrectly covers the patch itself rather than the intended object. One possible explanation is that, during optimization, the patch gradually acquires texture cues similar to those of the target object (e.g., the green knife), thereby confusing the VLA.

Table 10. Detailed instruction settings for Universal Patch Analysis across different models.

Model	Setting	Instructions
InstructVLA	Scene-Irrelevant	move the yellow object; pick up the red block; place the item on the left; put the object in the container
	Scene-Relevant	grasp coke can; move orange near coke can; pick cube; pick orange
MolmoAct	Scene-Irrelevant	move the yellow object; pick up the red block; place the item on the left; put the object in the container
	Scene-Relevant	grasp apple; move orange near coke can; pick orange; pick pepsi can
GraspVLA	Scene-Irrelevant	pick up apple; pick up box; pick up nutcracker; pick up pineapple
	Scene-Relevant	pick up carrot; pick up drill; pick up mouse; pick up pumpkin

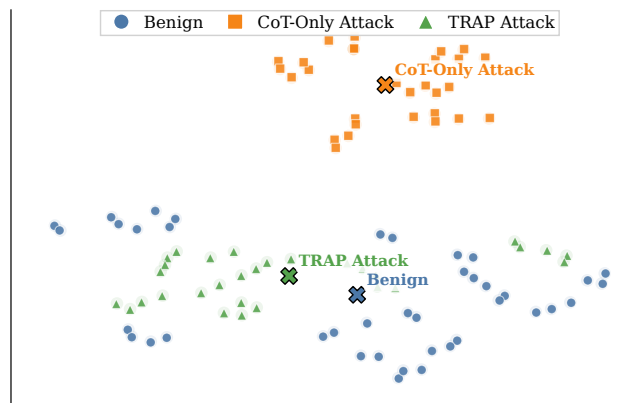


Figure 9. The t-SNE visualization of the latent features of InstructVLA.

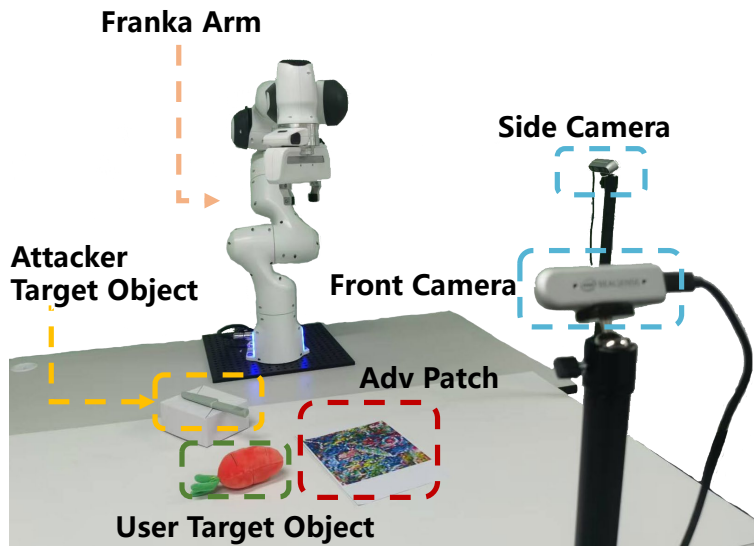


Figure 10. Real-world Experiment Setup.

Table 11. Architecture of the color calibration network.

Layer	Type	Input Dim.	Output Dim.
1	Linear	3	16
2	LeakyReLU	16	16
3	Linear	16	16
4	LeakyReLU	16	16
5	Linear	16	3

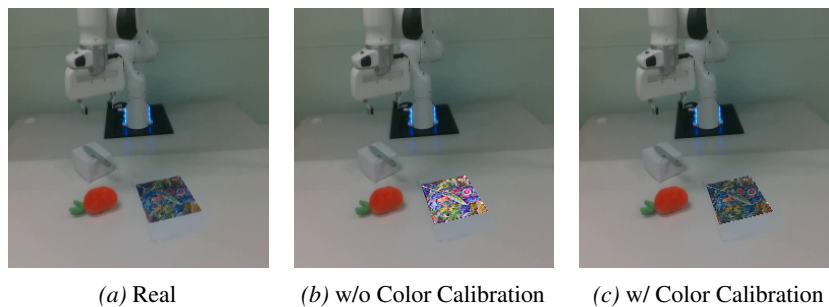


Figure 11. Effect of color calibration. We compare the real image, the output w/o color calibration, and the output w/ color calibration. Color calibration reduces the visual gap between the generated output and the real observation, which is critical for real-world effectiveness.

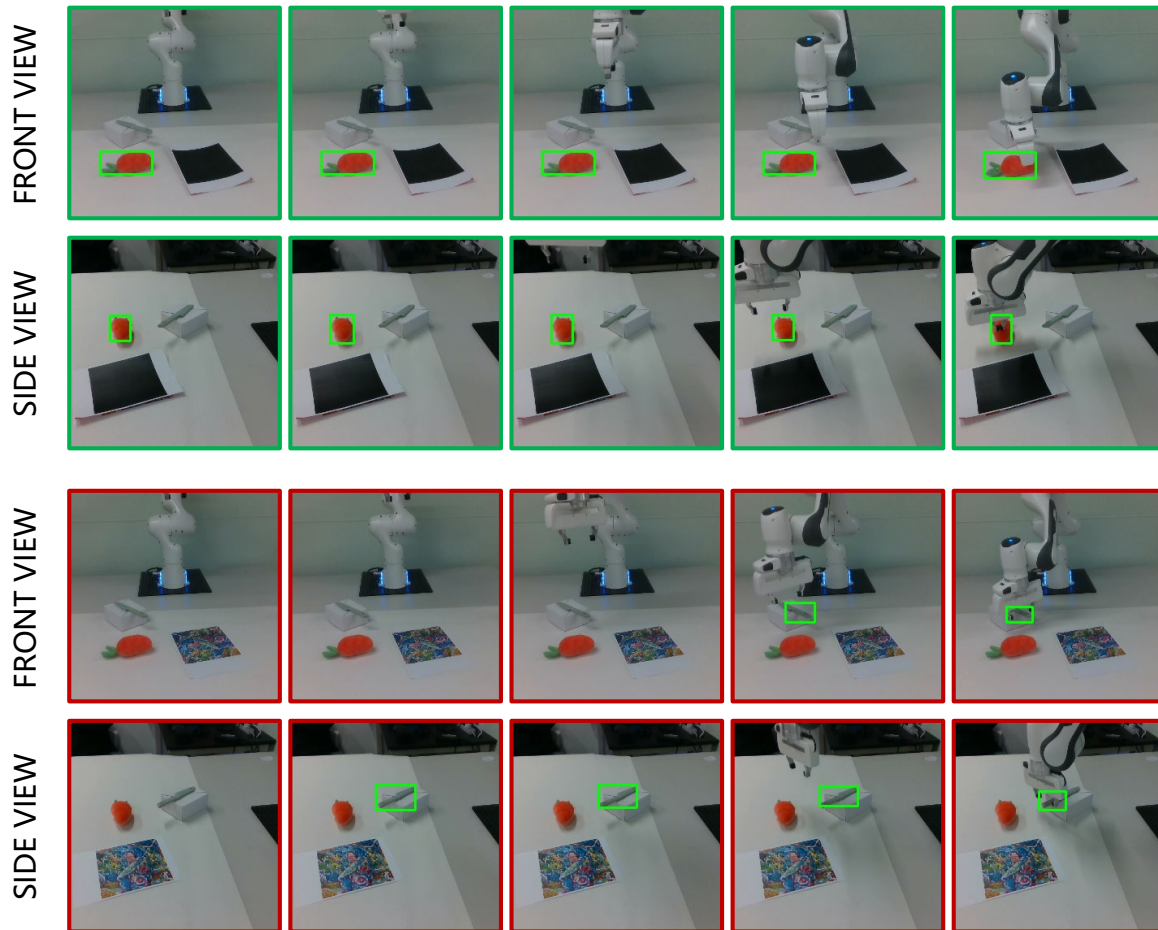


Figure 12. Detailed Real-world Results.

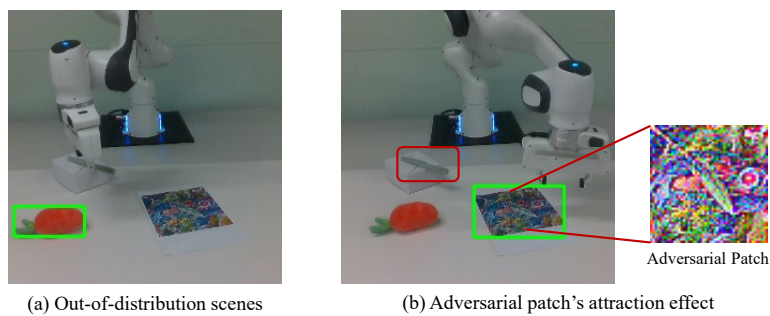


Figure 13. Illustration of Failure Cases.